Available online at www.sciencedirect.com
SCIENCE DIRECT®
Journal of Nuclear Materials 329–333 (2004) 958–962
journal of nuclear materials
www.elsevier.com/locate/jnucmat

Microstructural change in $AlMg_3$ alloy irradiated by spallation neutrons and high energy protons

D. Hamaguchi *, Y. Dai

Spallation Neutron Source Division, PSI, CH-5323 Villigen PSI, Switzerland

Abstract

An aluminum alloy Al–2.7wt%Mg ($AlMg_3$) has been used as the material for the safety-hull of the Swiss Spallation Neutron Source (SINQ) target. In the present work, the microstructure in the unirradiated and that from the beam window of the safety-hull has been investigated. For irradiated material, samples with two different doses (0.7 and 3.6 dpa) were investigated. In unirradiated material the dislocation density is not high, and are mainly located near precipitates. The sizes of the precipitates range from 10 to 200 nm in grain interior. Larger precipitates over 500 nm locate mainly along grain boundaries. After irradiation at around 60 °C, high density of small dislocation loops and helium bubbles were introduced. The bubbles distribute homogeneously inside grains at 0.7 dpa. At 3.6 dpa the size distribution shows a bimodal behavior. The bubbles at grain boundaries are larger than those in grain interior. The precipitates are partially amorphized after irradiation.

1. Introduction

Since aluminum–magnesium alloys are known to have good thermal conductivity, corrosion resistance, and, more importantly, very good radiation damage resistance, Al–2.7wt%Mg ($AlMg_3$) has been used as the material for the safety-hulls of the targets of the Swiss Spallation Neutron Source (SINQ). Former neutron irradiation studies on Al–Mg alloys revealed that addition of magnesium to aluminum leads to both enhanced formation of small dislocation loops and extension of the incubation period for cavity nucleation compared to that of pure aluminum [1–3]. They also suggested that the formation of fine scale Mg_2Si precipitates during irradiation played an important role on both suppression of cavity nucleation and irradiation hardening. An earlier 800 MeV proton irradiation study on Al–Mg–Si alloys, on the other hand, showed that the dissolution of the Mg_2Si precipitates during irradiation caused irradiation softening [4]. Since the results of tensile tests on the safety-hull of SINQ Target-3 also showed a substantial irradiation hardening and embrittlement of the material at the center of the beam window [5]. The present work, involving detailed TEM observation, was performed to investigate the microstructural change in the $AlMg_3$ alloy.

2. Experimental procedure

The composition of the $AlMg_3$ alloy used for the SINQ target safety-hull is listed in Table 1. The energy of the proton beam at the beam window of the safety-hull was 560 MeV and the maximum proton was about 3.2×10^{25} m^{-2}. The maximum irradiation dose including the neutron-induced contribution was about 3.6 dpa. Meanwhile, about 1125 appm helium and 1900 appm hydrogen were produced [6]. The irradiation temperature was around 60 °C. After irradiation, various samples were cut from the beam window for post-irradiation examinations. The samples for microstructural study were cut from two different places in the beam window. One was cut from the beam edge area, which is designated as 2A–R1, and the other was cut from the beam

* Corresponding author. Tel.: +41-56 310 5983; fax: +41-56 310 4529.
E-mail address: dai.hamaguchi@psi.ch (D. Hamaguchi).

0022-3115/$ - see front matter © 2004 Elsevier B.V. All rights reserved.
doi:10.1016/j.jnucmat.2004.04.291

Table 1
Chemical composition of the $AlMg_3$ for SINQ Target-3

Al	Si	Fe	Cu	Mn	Mg	Cr	Ti	Zn
Balance	0.30	0.25	0.03	0.35	2.72	0.04	0.01	0.04

center area, designated as 1A–R2. The maximum radiation dose in the beam edge area was about 0.7 dpa causing mainly from the neutron contribution, while it was about 3.6 dpa in the beam center area with both proton and neutron contributions. The microstructure was observed by using a JEOL-2010 TEM and a Zeiss DSM932 SEM. The EDX analytical method on both TEM and SEM were also used to estimate changes in chemical composition.

3. Results

3.1. Microstructure for unirradiated material

Fig. 1(A) and (B) show one SEM and one TEM micrographs of the unirradiated material. The main feature for unirradiated material is a relatively low density of both tangled dislocations and precipitates. The dislocation density for unirradiated material is about 2.1×10^{13} m^{-2}. It can be noticed that many dislocations are located at precipitates. The precipitates can be separated into three types with two different chemical compositions. The first is blocky precipitates that were revealed as silicon oxide SiO_2 from EDX analysis. These silicon oxides are mainly found along grain boundaries like precipitate '1' in Fig. 1(A). The other two types as those marked as '2' and '3' in Fig. 1(A), and are found both along grain boundaries and inside the grains. EDX analysis indicates that both types of precipitates have similar chemical compositions, which are rich in Fe, Mn, Cr, Si, and Al. The size of the precipitates in grain boundaries (type '2') are quite large compared to those in matrix (type '3'), that are often more than 500 nm with some exceeding 10 μm. The size of the precipitates in the grain interior, on the other hand, ranged from 10 to 200 nm. These small precipitates can be seen more clearly in Fig. 1(B).

3.2. Microstructure after irradiation

The microstructure changed significantly after irradiation. Irradiation induced a high density of small dislocation loops. At the same time, helium bubbles are also produced during irradiation. Fig. 2 shows the microstructure after irradiation in both samples: Fig. 2(A), (C) and (E) show the microstructure of sample 2A–R1 and Fig. 2(B), (D) and (F) show the microstructure of sample 1A–R2. The measured density and size of various defects are listed in Table 2.

The density of the loops was not significantly different in the two samples, although the sizes showed substantial difference. The mean size of the loop for sample 1A–R2 was about twice as large as the ones in sample 2A–R1. The size distribution for the loops is shown in Fig. 4. These loops were nucleated uniformly throughout the grains, but the presence of grain boundary denuded zone was observed in both samples. The denuded zone was much larger in sample 2A–R1 (about 220 nm) than that in sample 1A–R2 (about 90 nm).

The bubbles produced during irradiation showed quite different behaviors between both samples. There were high densities of small bubbles produced in both samples but the density of bubbles was 10 times higher in high dose sample 1A–R2 than that in low dose sample 2A–R1. In sample 2A–R1, the bubbles distributed nearly homogeneously in the matrix and the sizes of bubbles did not show a big difference, with a mean value around 2 nm. In sample 1A–R2, on the other hand, the size of the bubbles showed a bimodal behavior in the

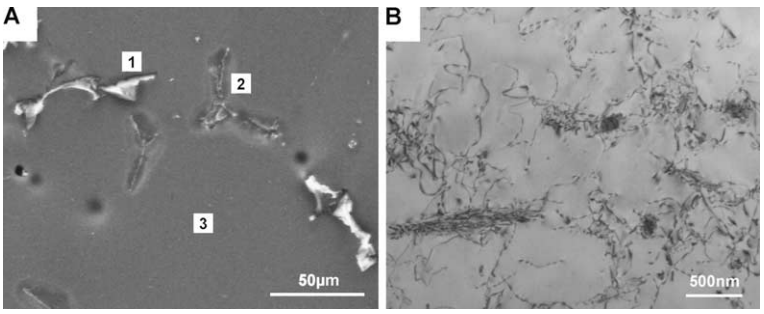

Fig. 1. The microstructure for unirradiated sample. A shows the SEM micrograph and B shows the microstructure observed by TEM.

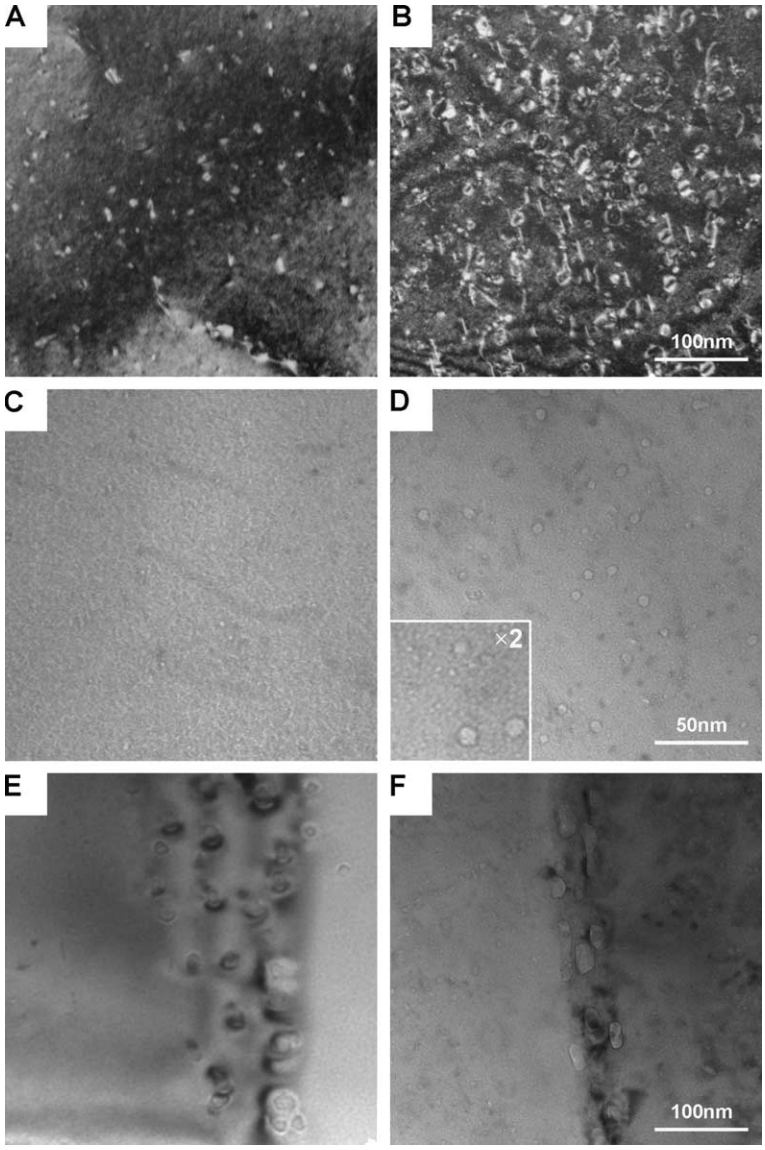

Fig. 2. The microstructure after irradiation. (A), (C) and (E) shows the microstructure for the sample 2A–R1 (0.7 dpa) and (B), (D) and (F) shows the microstructure for the sample 1A–R2 (3.6 dpa). The image taken near the $[1\,1\,0]_{Al}$ zone axis with $g = 200$.

Table 2
The density and average size of the loops and bubbles

	C_L (m^{-3})	S_L (nm)	C_B (m^{-3})	S_B (nm)	C_{GB} (m^{-2})	S_{BG} (nm)
2A–R1	2.5×10^{22}	6	1.2×10^{22}	2.3	9.9×10^{14}	15
1A–R2	3.0×10^{22}	14	1.5×10^{23}	2.5	9.5×10^{14}	33

C_L: loop density, S_L: average size of the loop, C_B: bubble density in matrix, S_B: average bubble size in matrix, C_{BG}: bubble density on grain boundary, S_{BG}:average size of the bubbles on grain boundary.

matrix. There were small bubbles around 2 nm and also large bubbles above 6 nm (Fig. 2(D)). The large bubbles were about 15% of the total bubble density. Many of these large bubbles were located in rows, which are probably along pre-existing dislocation lines. At grain boundaries, as seen in Fig. 2(F), there is a denuded zone

of ~120 nm wide for large bubbles, but not for small ones.

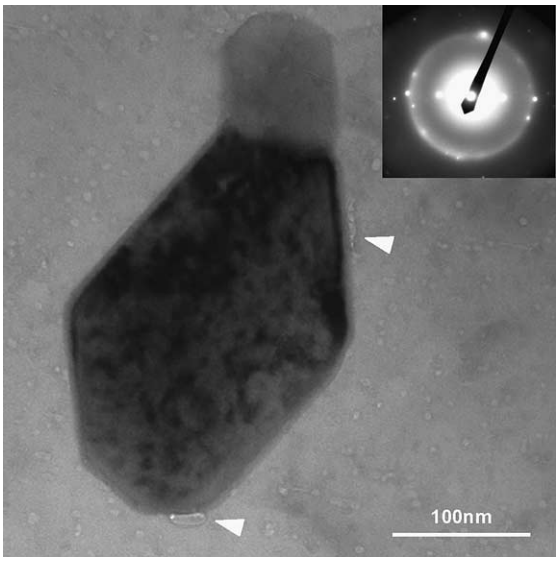

Fig. 3. The precipitate type '3' in the sample 1A–R2 after irradiation to 3.6 dpa. The arrows indicate an inhomogeneous distribution of the bubbles on precipitate-matrix boundary. The diffraction pattern illustrates that the precipitate become partially amorphous after irradiation.

The bubbles in grain boundaries were much larger than those in the grain interior, as shown in Fig. 2(E) and (F). The mean sizes are 15 and 33 nm for sample 2A–R1 and 1A–R2, respectively. In grain boundaries, the bubble are distributed nearly homogeneously while at the precipitate-matrix boundaries bubbles have inhomogeneous distributions, as indicated by the arrow in Fig. 3.

Irradiation also induced a change in the precipitates. Although the distribution and size of precipitates did not change in an obvious manner, they become partially amorphous after irradiation. Fig. 3 shows the micrograph and diffraction pattern of type '3' precipitates after irradiation. The EDX analysis indicates that the Si, Mn, and Fe content increased significantly in both type '2' and '3' precipitates, which were already rich in these contents. In the SiO_2 precipitates (type '1'), enrichment of only Si content is found. However, no indication of newly formed precipitates was found either in grain interior or in grain boundaries.

4. Discussions

Irradiation induced both dislocation loops and helium bubbles. Although the enhanced dislocation loop formation was also reported for neutron irradiations on

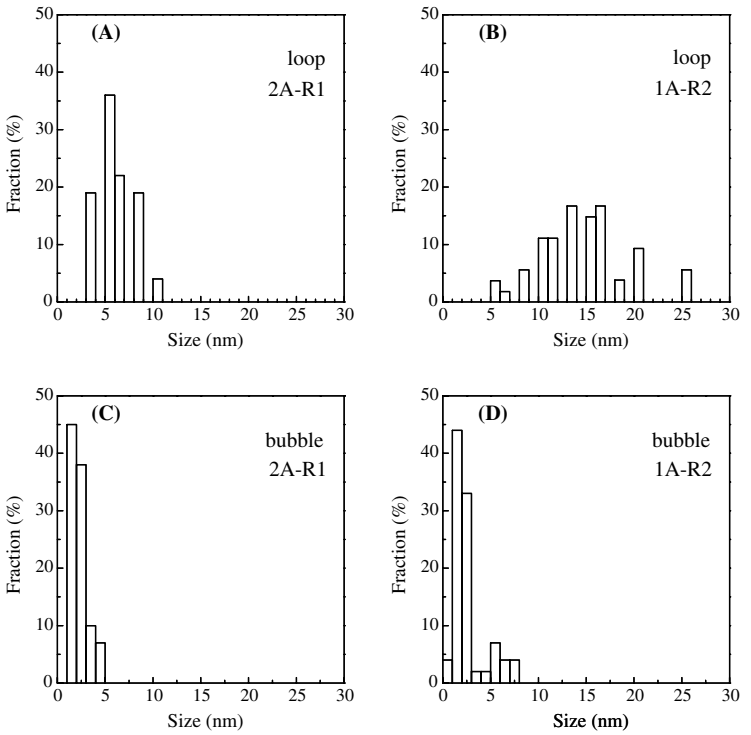

Fig. 4. Size distribution for the dislocation loops (A and B) and helium bubbles (C and D). (A) and (C) represent the result for the sample 2A–R1 (0.7 dpa) and (B) and (D) represent the result for the sample 1A–R2 (3.6 dpa).

Al–Mg alloys [1], the formation of the cavities in this study is much faster compared to the neutron irradiation case. Farrell reported that the incubation period for cavity formation in HIFR irradiation on 5052 Al–Mg alloy was up to 70 dpa [3]. While in the present study, the formation of the bubbles was already observed in the sample 2A–R1, where the corresponding irradiation dose was about 0.7 dpa. One reason for early nucleation of the bubbles in this study is the high helium production rate compared to that the neutron irradiations. Unfortunately the measured helium value is available only for the sample from the beam center area (1A–R2), the calculation by Lu et al. [7] shows good agreement with the measured helium concentration. The calculated helium production is about 130 appm for the sample 2A–R1, which gives a helium production rate of about 190 appm/dpa. This is about thousand times higher compare to former neutron irradiation cases. This high helium production rate would provide more nucleation site for the cavities compared to the neutron irradiation, which would significantly reduce the incubation period for the cavity nucleation. The influence of high helium production rate can also be seen in the sample 1A–R2, where the measured helium production is about 1125 appm that gives the helium production rate of about 300 appm/dpa. The bimodal behavior of the bubble size distribution and the higher density compared to the sample 2A–R1 indicate that there are more nucleation sites due to the higher helium production rate.

The former neutron irradiation studies on Al–Mg alloy suggested that the formation of fine scale Mg_2Si precipitates during irradiation caused by transmutation-produced Si leads to the extension of incubation period for cavity nucleation and growth [1–3]. At low doses, however, the amount of transmutation-produced Si is not sufficient to produce Mg_2Si precipitate. Farrell's study in HFIR irradiation also showed that no Mg_2Si precipitates were produced at the dose level of about 2 dpa, where the transmutation-produced Si level was about 5.8×10^{-2} at.% [3]. In this study, the precipitates were also not observed at the doses of about 3.6 dpa. This result agrees with Farrell's study. However, there was also no cavity formation found at this dose levels in neutron irradiation. Farrell and Houston suggested that a long incubation time for cavity nucleation may also be caused by low vacancy supersaturation due to trapping and recombination of interstitials and vacancies at solute atom [1]. However, they also showed that addition of Mg content in Al leads to an enhancement of dislocation loop formation under irradiation compared to pure Al. Under the proton irradiation condition where helium production rate is significantly high, and with a lack of sufficient Si content to produce Mg_2Si precipitates, Mg played more important role to produce high density of small dislocation loops instead of suppressing the cavity nucleation.

5. Conclusion

The Al–Mg alloy used in the safety-hull of SINQ target was examined after irradiation and the microstructure was compared to that prior to irradiation. The primary difference was the introduction of a high density of both dislocation loops and helium bubbles, the latter formed by the very high He/dpa ratio generated by the intense proton beam and accompanying spallation neutrons. The nucleation of the bubbles in this study is much faster compared to neutron irradiation. Significantly higher helium production rate compared to neutron irradiation is one of the reasons. A lack of sufficient transmutation-produced Si content to produce Mg_2Si precipitates during irradiation may also be the reason.

References

[1] K. Farrell, J.T. Houston, J. Nucl. Mater. 83 (1979) 57.
[2] R.T. King, A. Jostsons, Metal. Trans. A 6A (1975) 863.
[3] K. Farrell, J. Nucl. Mater. 97 (1981) 33.
[4] B.N. Singh, W. Lohmann, A. Ribbens, W.F. Sommer, Radiation-Induced Changes in Microstructure: 13th International Symposium (Part 1), in: F.A. Garner, N.H. Packan, A.S. Kumar (Eds.), ASTM STP 955, American Society for Testing and Materials, Philadelphia, 1987, p. 508.
[5] Y. Dai, H. Kaiser, K. Geissmann, G. S. Bauer, R. Zumsteg, H.P. Linder, F. Gröschel, PSI Scientific and Technical Report 2000, vol. VI, p. 33.
[6] Y. Dai, Y. Foucher, M.R. James, M. Oliver, J. Nucl. Mater. 318 (2003) 167.
[7] W. Lu, M.S. Wechsler, Y. Dai, J. Nucl. Mater 318 (2003) 176.